Improving the accuracy of PEPT algorithms through dynamic parameter optimisation

Herald, Matthew; Sykes, Jack; Parker, David; Seville, Jonathan; Wheldon, Tzany; Windows-Yule, Christopher

DOI:
10.1016/j.nima.2022.167831

Document Version
Publisher's PDF, also known as Version of record

Citation for published version (Harvard):
Herald, M, Sykes, J, Parker, D, Seville, J, Wheldon, T & Windows-Yule, C 2023, 'Improving the accuracy of PEPT algorithms through dynamic parameter optimisation', *Nuclear Instruments & Methods in Physics Research. Section A. Accelerators, Spectrometers, Detectors*, vol. 1047, 167831.
https://doi.org/10.1016/j.nima.2022.167831

Nuclear Inst. and Methods in Physics Research, A 1047 (2023) 167831

Contents lists available at ScienceDirect

Nuclear Inst. and Methods in Physics Research, A

journal homepage: www.elsevier.com/locate/nima

Improving the accuracy of PEPT algorithms through dynamic parameter optimisation

Matthew Herald [a,*], Jack Sykes [b,a], David Parker [b], Jonathan Seville [a,c], Tzany Wheldon [b,c], Christopher Windows-Yule [a,c]

[a] School of Chemical Engineering, University of Birmingham, Birmingham, United Kingdom
[b] School of Physics and Astronomy, University of Birmingham, Birmingham, United Kingdom
[c] Positron Imaging Centre, University of Birmingham, Birmingham, United Kingdom

ARTICLE INFO

Keywords:
PEPT
Compton scattering
Monte Carlo
GATE
Digital-Twin

ABSTRACT

Positron emission particle tracking (PEPT) is used to study a wide range of scientific, industrial, and biomedical systems, typically those inaccessible through conventional optical particle tracking techniques. However, in dense or thick-walled systems a fraction of the coincident gamma-rays emitted from a PEPT tracer, called Lines-of-Response (LoRs), are attenuated via Compton scattering. Additionally, at high source activity, random LoRs may be formed by two unrelated events. The incorporation of scattered or random LoRs decreases PEPT spatial accuracy and can distort the trajectory. In this work, we use validation experiments and simulations to investigate the spatial accuracy of the Birmingham Method (BM) PEPT algorithm when two key free parameters are changed: the total number of LoRs in the sample and the fraction of LoRs in the sample used to locate the tracer. Our results show that the default algorithm parameters are not suitable for all cases, however, Monte Carlo simulations of PEPT experiments can be used to estimate the optimal parameter values. Ultimately a variant of the BM, called Dynamic-BM, is demonstrated in a virtual PEPT experiment. Dynamic-BM uses the optimal parameters on a sample-by-sample basis improving PEPT accuracy in this case by 4.03% over the best constant parameters and 76.5% over the default parameters. These improvements make PEPT a more accurate and thus more useful tool.

1. Introduction

Many types of systems used in scientific, industrial, and biomedical applications pose a challenge for those who study them since the internal dynamics of fluids and solids are often difficult to observe directly. This is because the materials themselves are opaque, they are inaccessible behind the system's opaque walls or both. To better understand what is happening inside these systems, a fully three-dimensional, Lagrangian particle tracking technique called positron emission particle tracking (PEPT) was developed [1]. The PEPT technique locates a quasi-point, positron-emitting tracer by detecting coincident 511 keV gamma-rays generated from positron-annihilation [2]. Using samples on the order of 100 of these rays, which are termed lines-of-response (LoRs), the location where the LoRs converge is determined to be the tracer's position. Tracers are tracked over time using subsequent samples of LoRs to develop a trajectory. The PEPT technique is similar to positron emission tomography (PET), in so far as it uses the same types of tracers and detectors, but where PET produces images of the 3-dimensional radio-nuclide concentration throughout the imaging volume at a low temporal resolution (<1 Hz), PEPT assumes a quasi-point tracer and returns the 3-dimensional centre of the discrete tracer's radio-nuclide distribution at a comparatively high temporal resolution (>100 Hz) [3]. This allows PEPT to extract information from systems such as the velocities of individual tracers, granular temperature, and flow dynamics in engineering systems that PET cannot provide. In the decades of research since PEPT was first introduced, PEPT has been shown to capture tracer trajectories with high spatiotemporal resolution and used to study a wide range of systems [4]. For example, PEPT has been used to characterise flow regimes in gas-fluidised and vibro-fluidised beds, analyse the shape and behaviour of granular beds in rotating drums, and measure the Reynolds stress and turbulent kinetic energy budget in pipe-flow [5–8]. The basic principle of PEPT is shown in Fig. 1.

Ideally, all of the LoRs should lead back to a single point which is the tracer location and these are termed 'true' LoRs [9]. However, LoRs may also be 'scattered' or 'random'. Scattered LoRs are formed when one or both gamma rays in an LoR undergo scattering before reaching the detector. The most common type of scattering for 511 keV gamma-rays is Compton scattering, which is an inelastic scattering process that occurs when a photon interacts with an electron, lowering

* Corresponding author.
E-mail address: mxh1092@student.bham.ac.uk (M. Herald).

https://doi.org/10.1016/j.nima.2022.167831
Received 29 April 2022; Received in revised form 9 November 2022; Accepted 15 November 2022
Available online 22 November 2022

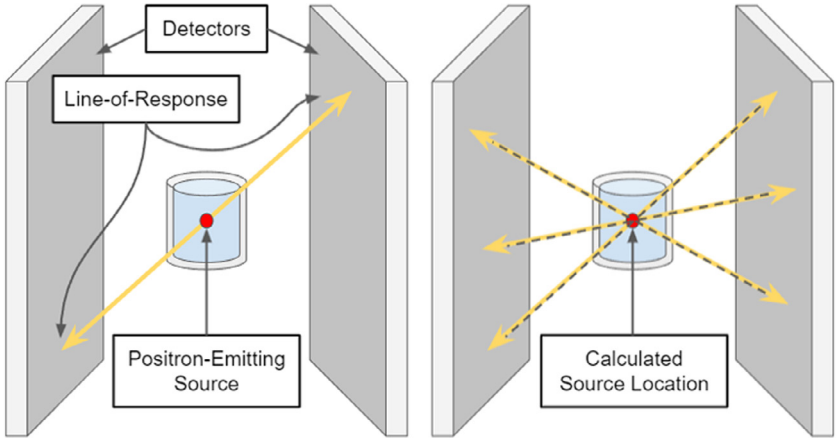

Fig. 1. 511 keV gamma-rays are collected using two opposing radiation detectors and form an LoR (left). When processed with a PEPT algorithm, the LoRs reveal the tracer location (right).

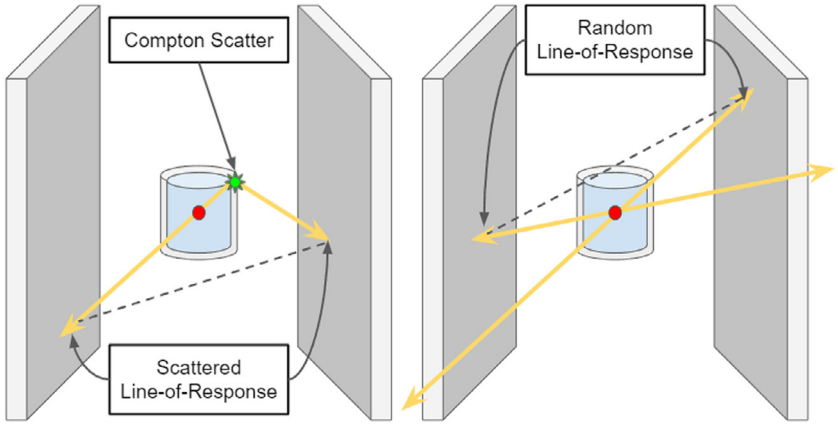

Fig. 2. A scattered LoR is formed when one or both gamma rays undergo Compton scatter (left). A random LoR is formed when two unrelated gamma rays are detected within the coincidence window (right).

the energy of the photon and changing its direction [10,11]. A scattered LoR, shown in Fig. 2, does not intersect the source location and is therefore corrupted for PEPT. While 511 keV gamma-rays are much more penetrating than visible light and X-rays, like all forms of electromagnetic radiation, they exponentially attenuate. For a beam of 511 keV gamma-rays with initial intensity I_0, the amount that penetrates without attenuating is dependent only on the material thickness, Δx, and the linear attenuation coefficient, μ, as shown in Eq. (1) [12].

$$I = I_0 \exp(-\mu \Delta x) \tag{1}$$

A 'random' LoR may also be formed between two unrelated events within the energy window. Since the two gamma rays in a random LoR originate from separate positron annihilations, the LoR is corrupt and will not intersect the source location. The rate of random LoRs is predictable and determined by the count-rate of individual 'singles' events between two detectors, S, and the coincidence window, τ, shown in Eq. (2) [13]. Since the rate of random LoRs squares with the singles rate, at high count-rates random LoRs may form a large fraction of the LoRs in a sample. A diagram of a scattered and random LoR is shown in Fig. 2.

$$R = 2\tau S_1 S_2 \tag{2}$$

The Birmingham Method (BM) PEPT algorithm was designed with the fact in mind that many LoRs in a sample may be corrupted, thus only a fraction of the LoRs in a sample should be used to find the tracer position [2]. The BM works by minimising the sum of the distances of an estimated tracer position to each LoR in the sample, described by Eq. (3), where $D(N)$ is the sum of all the distances in the sample of LoRs, N, and $\delta_{LoR}(m)$ being the three-dimensional distance of an individual LoR to the estimated tracer location, m [8]. Once the tracer position is estimated and the distances of LoRs to the position known, the LoR furthest from this point is removed and the remaining LoRs are recycled to update the estimated position. This iterates until only a user-specified fraction of the LoRs remain, f. This process is shown in Fig. 3. The BM has two free parameters: the fraction of the LoRs remaining in the initial sample, f, and the total number of LoRs in a sample, N_{LoRs}. The default parameters of the BM are 0.05 and 250 for f and N_{LoRs}, respectively. These parameters are conservative so that they can be applied to many different systems and produce reasonable trajectories.

$$D(N) = \sum_{N} \delta_{LoR}(m) \tag{3}$$

It is known that thicker and denser systems will cause more scattered LoRs and that more active tracers will cause more random LoRs. However, little has been done to develop ways to understand how this affects PEPT measurements and, further, predict the values for f and N_{LoRs} which will maximise the spatial accuracy of the BM. In recent work, a method to find the optimal N_{LoRs} has been proposed [14]. This method relies on using a large enough sample to give adequate statistics but is limited such that the tracer does not move significantly compared to the measurement uncertainty during the time used to locate the tracer. This can be summarised in Eq. (4), where w is a detector-specific parameter for spatial resolution, R is the detection rate of LoRs, and v is

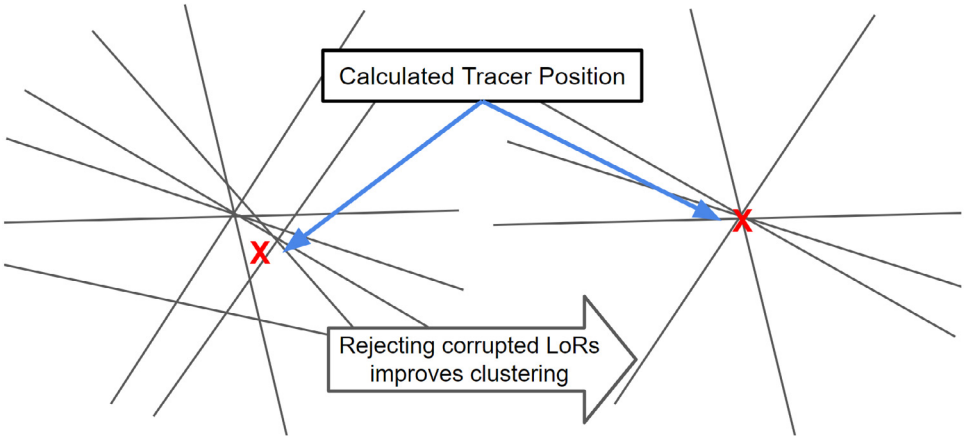

Fig. 3. A sample of LoRs and the initial guess for the tracer position (left). After a fraction of the LoRs furthest away from the initial guess are removed, the remaining LoRs are re-clustered for a more accurate position (right).

the tracer velocity. However, this approach can only be used accurately if the tracer velocity and f are known, which is often not the case.

$$N = f^{\frac{-1}{3}} \left[\frac{Rw}{v}\right]^{\frac{2}{3}} \tag{4}$$

In this work, we use PEPT measurements and simulations to investigate how the spatial accuracy of the BM is affected by the parameters f and N_{LoRs} under a range of experimental conditions, including both stationary and moving tracers. In addition to real experiments, a Geant4 Application for Tomographic Emission (GATE) v 9.1 model of the ADAC Forte, validated to within 10% of experimental measurements, is used to recreate the experiments [15,16]. These serve as further validation for the model and are later expanded to test a range of conditions not explicitly considered during the experiment. The values for f and N_{LoRs} which maximise the spatial accuracy for each PEPT trajectory are extracted as a function of the tracer position. To utilise this information, a new version of the BM, called the Dynamic-BM (DBM), is developed which dynamically changes the fraction of LoRs remaining in the sample and the sample size of LoRs based on an estimate of the tracer position found using non-optimal parameters. This new method is expected to provide both higher spatial and temporal resolution than the original BM algorithm since it can use the optimal parameter combination on a sample-by-sample basis. Moreover, this removes the necessity for trial and error optimisation as well as the cost this engenders and provides a justifiable reason why certain parameters were chosen.

2. Methods

Two experiments are created to investigate how N_{LoRs} and f vary under different conditions. The first experiment consists of low-activity, static tracers placed in the centre of the ADAC Forte dual-headed positron camera. This system is depicted in Fig. 4. The tracer is surrounded by a cylinder of material to induce Compton scattering. The experiment is repeated with six materials detailed in Table 1; this shows how the fraction of corrupted LoRs affects the optimal f parameter. The second experiment is a moderately high-activity tracer fixed to the end of an impeller rotating at 100 RPM in an attritor mill. The BM is used with a range of f and N_{LoRs} to track the tracer, and then the PEPT trajectories are compared to the predicted tracer position based on the known rotation rate and initial position to calculate the mean spatial error. The combination of parameters that maximises the mean spatial accuracy of the trajectory is found. This shows how the optimal N_{LoRs} is affected by tracer motion.

Both the static tracer experiments and the attritor mill experiment are recreated in GATE to serve as validation of the model. Subsequently, the GATE model of the attritor mill is then used again to place the tracer in a range of possible initial positions which will result in different fractions of corrupted LoRs and a range of tracer velocities. Each trajectory is analysed using the BM and the optimal parameter combination is extracted as a function of the tracer position. Ultimately, these virtual PEPT experiments are used to observe how f and N_{LoRs} change throughout the attritor mill system and are used to develop the DBM algorithm. The performance of the DBM will be compared to the best constant parameters and also the default algorithm parameters.

2.1. Static tracer experiment

A small tracer, on the order of the range of positrons in the material and PEPT uncertainty, should be used to ensure the detected LoRs form a tight cluster near the tracer. The tracer chosen for this experiment is a 1 mm diameter sphere of anion exchange resin labelled with fluorine-18 (F-18). F-18 is an ideal positron-emitting isotope for PEPT because it has one of the lowest energy spectra for positrons and thus a low range [17]. The anion exchange resin adsorbs F-18 ions from a solution of radioactive water produced on-site at the Positron Imaging Centre [18]. On the day of the experiment, the tracer was activated with an initial activity of 2.8 MBq and placed inside a 0.5 ml plastic vial for handling. According to a recent characterisation of the ADAC Forte, a tracer of 2.8 MBq will produce less than 5% random LoRs, meaning nearly all LoRs not intersecting the tracer location will most likely have undergone Compton scattering before being detected [15].

To attenuate the 511 keV gamma-rays, the vial is placed in the centre of an 800 ml cylindrical glass beaker filled to 500 ml with bulk density attenuating material. The inner diameter of the beaker is 100 mm and filled to the height of 65 mm, confirming that a volume of material of approximately 500 ml is used. The wall thickness of the beaker is 5 mm. Once filled, the beaker's mass was measured. The initial mass of the beaker was subtracted to find the total mass of the attenuating material. The density of the materials, ρ, is calculated by dividing the mass by the volume. The materials and their properties are listed in Table 1. Materials like air and high-density polyethene (HDPE) have low linear attenuation coefficients, μ, while steel and copper have larger coefficients, meaning they will attenuate a larger fraction of the gamma rays [11]. A small sample of some of these materials and the filled beaker is shown in Fig. 4. The fact that materials are bulk and porous is not expected to have an effect in this experiment since the diameters of the materials are much smaller than the diameter of the beaker. The attenuation of gamma rays in this experiment will approximate those of a perfectly continuous attenuation medium.

During the experiment, the beaker is placed in the centre of the field of view (FOV) of the ADAC Forte. The Forte is a dual-headed positron camera used for PEPT at the Positron Imaging Centre and is the most extensively used detector system for performing PEPT experiments [8,

Fig. 4. A small sample of four of the materials used to induce attenuation (left). From left to right: steel, copper, glass, and MCC. The beaker is filled with steel balls and the source is placed in the centre of the field-of-view (FOV) of the Forte (right).

Table 1
List of the bulk materials and their attenuating properties [11].

Material	ρ_{bulk} (g/cm^3)	μ/ρ_{bulk} (cm^2/g)	μ (cm^{-1})	Attenuation (%)
Air	0.00129	0.0806	0.000111	19.4
HDPE	0.890	0.0931	0.0828	64.8
MCC	1.421	0.0915	0.130	78.0
Glass	1.661	0.0858	0.143	80.7
Steel	4.425	0.0832	0.368	98.0
Copper	5.025	0.0827	0.415	98.7

19,20]. It is comprised of two opposing large-area sodium iodide crystals, 16 mm thick, each with an active area of 380 × 510 mm [15]. The intrinsic efficiency of the Forte is reported to be approximately 23% and it has an energy resolution of 14% [15]. Ideally, an energy window should be set as narrowly as possible around 511 keV, to exclude photons that have Compton scattered [21], but broad enough not to exclude valid annihilation pairs. The energy window is set to 50% to capture all true LoRs, yet inevitably recording some scattered LoRs which can later be discarded by the Birmingham algorithm. The two heads of the Forte have an adjustable separation and for this experiment are set to their maximum separation of 800 mm to achieve the most uniform illumination. Each material is imaged until more than 1,000,000 LoRs have been collected, which is enough to locate the tracer several times using the BM across a range of N_{LoRs} in the sample size. Since the position of the tracer is not known exactly, the standard deviation of the PEPT detected position, the PEPT precision, σ, is used to quantify the performance of different f and N_{LoRs} parameter combinations. This is calculated using Eqs. (5) and (6), which is the three-dimensional standard deviation of the detected positions.

$$\sigma_x = \sqrt{\frac{\Sigma(x_i - \bar{x})^2}{N}} \tag{5}$$

$$\sigma = \sqrt{\sigma_x^2 + \sigma_y^2 + \sigma_z^2} \tag{6}$$

2.2. Moving tracer experiment

In previous work, the spatial accuracy for *static* tracers has been shown to improve when more LoRs are used per sample [22]. However, in real PEPT experiments, the tracer typically moves throughout the system. This movement limits the N_{LoRs} per sample if the tracer moves more than a few millimetres between the detection of the first and last LoRs in the sample. If the tracer moves more than this, particularly if the tracer is changing direction or accelerating, the PEPT-detected position will incur higher spatial errors [2,23]. Thus there should always exist an optimum N_{LoRs} per sample for a given system at a given point in time.

To investigate this in a system representative of a PEPT experiment, an attritor mill is placed near the centre of FOV and a tracer is fixed to the end of the impeller as it rotates in the mill at 100 RPM. Mills of this type are used across a wide range of industrial and pharmaceutical applications and have been studied in the past using PEPT [24,25]. Due to the thick steel walls and predictable circular rotation of a particle fixed to the impeller, this system is an ideal candidate to investigate the effect of N_{LoRs} on the spatial accuracy of the BM. In other work, similar rotating systems have been used to better understand how changing the parameters f and N_{LoRs} affects PEPT measurements [2,26]. The attritor mill and a schematic of the mill dimensions are shown in Fig. 5.

The tracer used for this experiment is a 1.2 mm diameter MCC bead activated with a solution of F-18 and water to an initial activity of 22 MBq. A tracer of this activity is ideal for PEPT experiments in the Forte since this is approximately the activity which will produce the highest true LoR count-rate before dead-time and random LoRs degrade the measurement [15]. This tracer is taped to the end of the upper impeller in the attritor mill at a radius of 63 mm. At 100 RPM the tracer will rotate at a constant velocity of 660 mm/s. The mill is then placed near the centre of the FOV of ADAC Forte at a head separation of 510 mm. The mill is imaged over approximately 1 min (i.e. 100 rotations) to be able to develop good statistics of the tracer locations as it rotates.

To assess the performance of different f and N_{LoRs} combinations using the BM, first, each directional component of the PEPT trajectory is fitted to a sinusoidal equation as a function of time, t, as shown in Eq. (7). The amplitude, A, in the x and z components should be approximately 63 mm and in the y component, 0 if the mill is perfectly oriented with respect to the detector axes. Since the mill is likely not perfectly level a sinusoidal equation is fit to the y-component as well. The rotation rate, ω, is approximately 100 RPM, and ϕ is the phase shift which depends on the initial position of the tracer. The PEPT deviation from this motion is calculated by comparing each PEPT detected position to the predicted position using the fitted equations. In this way, the mean spatial error of the trajectory is calculated using Eqs. (8) and (9).

$$x_{Fit}(t) = A\sin(\omega t + \phi) + c \tag{7}$$

$$\varepsilon_{x_i} = |x_{PEPT_i} - x_{Fit_i}| \tag{8}$$

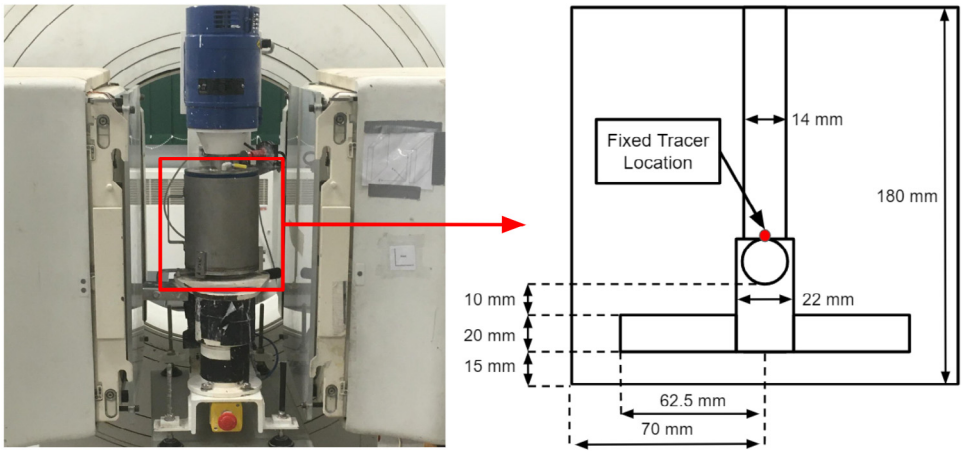

Fig. 5. The attritor mill near the centre of the FOV of ADAC Forte (left). A schematic of the dimensions of the mill and the tracer fixed to the impeller (right).

$$\epsilon = \frac{1}{N}\sum_{i}^{N}\sqrt{\epsilon_{x_i}^2 + \epsilon_{y_i}^2 + \epsilon_{z_i}^2} \tag{9}$$

2.3. Monte Carlo model

GATE v 9.1 is a powerful tool used to simulate radioactive sources, detectors, and geometries commonly found in medical imaging and radiotherapy applications [27]. PEPT relies on the same equipment as in medical imaging, thus GATE can reliably be used to create virtual PEPT experiments without having to extend the existing toolkit [22,28]. The GATE model of the ADAC Forte used in this work has been validated using a characterisation of the detector when it was installed at the Positron Imaging Centre and calibration experiments following an industry-standard protocol, showing agreement between simulation and experiment to within 10% across all tested metrics [15]. The model includes all of the major structural components of the ADAC Forte such as the sodium-iodide scintillation crystal, back compartment, and cover around the detector heads. The model also includes the 'digitizer' which is based on the pulse-processing stages of the detector, crucial for replicating the spatial resolution, sensitivity, and count-rate response of the detector [29].

The ADAC Forte's digitizer is responsible for converting the interactions of the simulated gamma-rays with the scintillation crystals, termed 'hits', into a 'pulse' which is analogous to what would be produced by the real detector by passing the time, position, and energy of the hit through blurring filters. This is needed because the simulation produces exact values, but in reality, some characteristic imprecision is present. A flow diagram of the ADAC Forte's digitizer is shown in Fig. 6. Once the hit is registered, the information from the interaction such as the time, position, and energy absorbed by the crystal is recorded as a GATE pulse. Next, a series of blurring filters are added to match the time resolution, spatial resolution, and energy resolution of the detector. In the simulation, the values for these pulse properties are known absolutely and must be blurred to mimic the imprecision of real detectors. Next, the pulses which fall near to each other in a short time window of 400 ns are allowed to pile-up on one another forming a combined signal. After this step, energy thresholds for recording the pulse are added which ensures that only pulses falling within the threshold will trigger a detector response, excluding pulses below 250 keV and 950 keV. Pulses falling within this range trigger the detector to record them and this creates a period where no pulses can be recorded called dead-time. The dead-time model used for the single pulses is a paralysable model with a dead-time of approximately 1.2 μs which can be restarted by another pulse [30]. Of the recorded singles pulses, only those falling within a 50% energy window of the 511 keV photo-peak, which is 360 keV to 640 keV, are considered for forming a coincidence

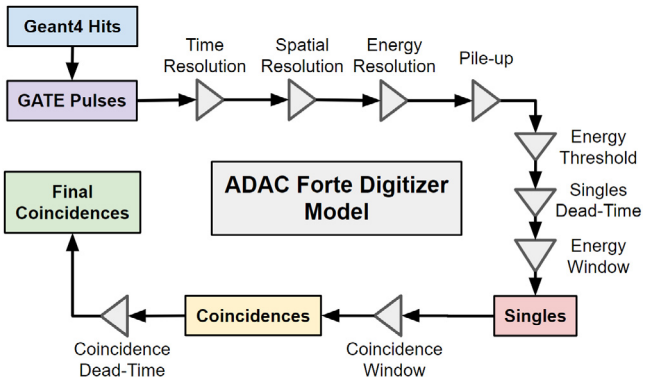

Fig. 6. The ADAC Forte's digitizer is represented as a flow diagram of the pulse-processing stages.

if another pulse on the opposite head of the detector records a single within the coincidence window of 15 ns. Finally, from the coincidences that are formed, an additional non-paralysable coincidence dead-time of 1.2 μs is used to filter the data following the data write speed limitation of the detector, which forms the final coincidences. These final coincidences are what are ultimately considered the LoRs which are used for PEPT [15].

This GATE model of the ADAC Forte is first used to repeat the experiments described in Sections 2.1 and 2.2 for comparison and further validation. After this, the GATE model and recreated attritor mill are used to expand the tested conditions to observe how the optimal combination of f and N_{LoRs} changes throughout the system. These optimal parameters are used in Section 2.4 to develop the DBM algorithm.

2.3.1. Static tracer simulation

Following the previously described experiments, the tracer, geometry, and detector for the static tracer experiments are replicated in GATE. This starts by creating a radioactive tracer defined as a 1 mm diameter resin sphere, emitting positrons with an F-18 energy spectrum. The tracer is placed inside a geometric model of the glass beaker which has been filled with 500 ml of bulk-density material. A cross-section of the beaker and source geometry is shown in Fig. 7. To replicate the attenuation of each material, new material definitions are added to the GATE material database which is described in Table 1. The tracer is prescribed an activity equal to that of the tracer's activity at the beginning of each data acquisition. Initially, the tracer was approximately 2.8 MBq at 11:48 am, but by the end of all experiments

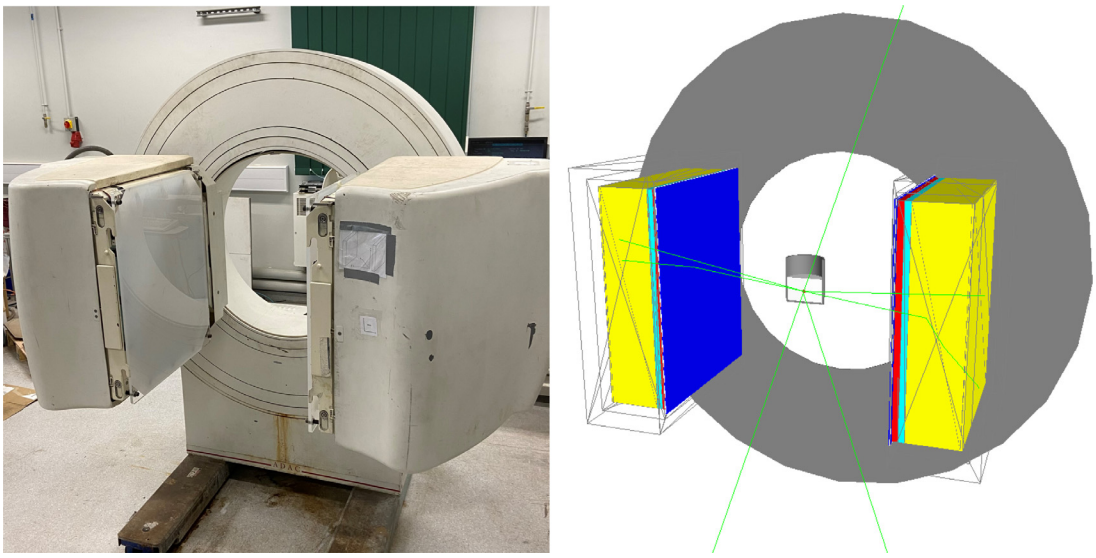

Fig. 7. The ADAC Forte dual-headed positron camera at the Positron Imaging Centre (left). GATE model of the Forte with a cutaway of the experimental geometry and source in the centre of the FOV (right).

decayed to approximately 1.3 MBq. For each simulation, the activity is adjusted accordingly to compensate for decay. Finally, the tracer and beaker are placed in the centre of the FOV of the GATE model of the ADAC Forte. The detector separation is set to 800 mm. While the exact positions of the tracers simulated in GATE are known, Eq. (6) is still used to calculate the PEPT precision to compare the real experiment and simulations directly.

2.3.2. Moving tracer simulation

In a similar manner as before, the moving tracer experiment is recreated in GATE. The model of the ADAC Forte is the same as the model used for the static tracer experiment and the head separation is set to 510 mm, which is as close to the system as the detectors could be set. A lower head separation results in higher geometric efficiency, meaning LoRs can be collected at a higher rate. At the time of the experiment, the tracer was measured to approximately 20 MBq. This is modelled in GATE as a 1.2 mm diameter sphere emitting positrons with an F-18 energy spectrum.

The mill dimensions can be found on the right-hand side of Fig. 5 and the GATE model of the mill is shown in Fig. 8. It consists primarily of a 70 mm diameter vessel lined with polyethylene and a stainless-steel impeller with 4 pins. The polyethylene liner is 10 mm thick and the outer stainless-steel wall is 5 mm thick. The inside of the vessel is filled with air to match the experimental conditions. In a real experiment, the mill will be filled with grinding material. To recreate this in GATE, the model could be filled with a volume of the bulk density material, or a Discrete Element Method simulation can be used to calculate the three-dimensional density distribution and this can be imported into the simulation using a voxel array [23] (see Fig. 8).

The whole mill is rotated about the y-axis at 100 RPM to induce particle motion. This is achieved through discrete rotations of every simulation time-step of 0.0005 s. For the tracer fixed at a 63 mm radius, this results in a change in position of approximately 0.33 mm per time-step. This is smaller than the tracer diameter and can thus be safely used to mimic continuous tracer motion. The GATE simulation produces LoRs which are processed in the same way as real PEPT data. A range of different f and N_{LoRs} are used to locate the tracer. The PEPT trajectory is then compared back to the GATE-prescribed tracer positions using Eqs. (7)–(9). The GATE simulated tracer's position is known exactly and there is no variability in its rotation rate or system vibration present. As such, the spatial accuracy of the GATE simulated tracer is expected to be somewhat higher than in the real experiment.

2.4. Dynamic Birmingham Method

In PEPT experiments, the scattering environment and detector sensitivity change as a function of the tracer position. The amount of corrupted LoRs in a sample affects the optimal f while the sensitivity affects the optimal N_{LoRs}. However, the BM uses constant parameter values. This means users must choose a conservative parameter combination that will work over the whole data set. Inevitably, this will return trajectories with lower spatial accuracy than is theoretically possible. To solve this problem, a variant of BM is developed called Dynamic-BM (DBM), 'Dynamic' because it can dynamically change f and N_{LoRs} to the optimal values determined by a Monte Carlo simulation of the experiment as the tracer moves through the system.

Initially, the DBM uses constant values of f and N_{LoRs} to estimate the position of the tracer. Then, for each initially-estimated tracer position, the optimal parameter values are looked up from a table produced by Monte Carlo simulation. To use this table, the predicted 3-dimensional location of the tracer and other optional information is input, then the closest simulated position is found and the optimal parameters are output. This approach relies on the user simulating a sufficiently high number of possible tracer positions within the system such that the change in parameter values between adjacent simulated positions is smooth. The Monte Carlo simulations must be analysed before using the DBM to generate the optimal parameter look-up table.

To test the DBM, the attritor mill is simulated using GATE with the tracer placed in a range of initial positions. This is done to investigate the whole system's behaviour rather than only a single region. To match the experimental conditions, the mill is rotated at 100 RPM and the tracer activity is set to 22 MBq. Each tracer position is a new GATE simulation. The initial tracer positions are seeded in one quadrant of the mill to take advantage of the symmetry of the system. The positions are created in regular intervals in the x and z direction from 0–60 mm in 20 mm steps and the y-direction from −50–50 mm in 12.5 mm steps. The positions falling outside of the system or intersecting the impeller are removed, leaving a total of 84 positions. Since the impeller is rotating the position of the tracer is important for the optimal f and N_{LoRs} values since it will cause different amounts of scattering depending on its rotated angle. In the simulation, the rotation of the impeller is prescribed so it is known, but during a PEPT experiment, this can be more difficult to ascertain. However, the ADAC Forte can record readings from an optical switch directly into the data file, allowing the impeller rotation angle to be recorded throughout an experiment [31].

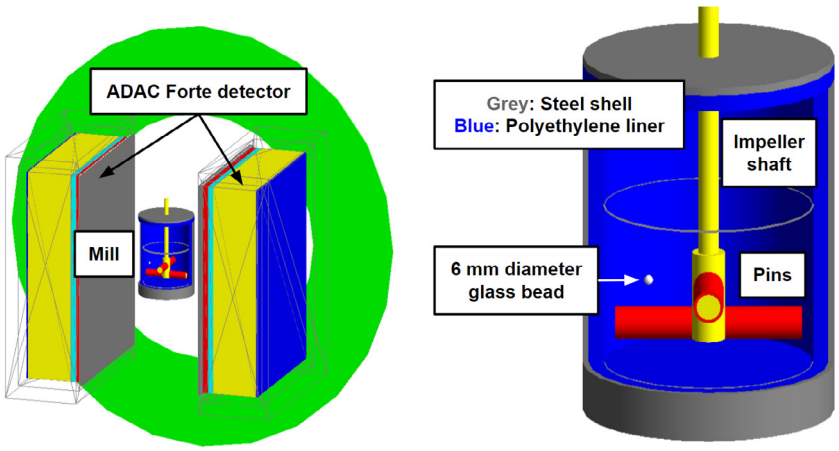

Fig. 8. The GATE model of the ADAC Forte dual-headed positron camera (left) and a cut-away of the attritor mill (right). In the cut-away, the major components are labelled.

The 360° is divided into 30° increments and the optimal f and N_{LoRs} are calculated over this range.

To use the look-up tables, first, the amount the mill is rotated must be determined. This is done by multiplying the time by 360° and dividing by the rotation period, 0.6 s. Since all rotations beyond 360° are duplicates of previous rotations, a modulo operation is performed. Then all the simulated positions within the nearest rotation are compiled and the values of f or N_{LoRs} for the position closest to the PEPT estimated position are extracted. Using this method, the optimal f and N_{LoRs} of any point within the system can be determined. Due to the change in N_{LoRs} per sample, the number of detected positions in a trajectory processed using the BM and the DBM may vary. To ensure the changing parameters are used at the appropriate position within the data set, the f and N_{LoRs} are linearly interpolated as a function of time and the average time of the LoRs in each sample is used to compute the exact parameter values.

To assess the performance of the DBM, it is compared to both the default BM parameter values of 0.05 f and 250 N_{LoRs} as well as the best constant parameter values. This represents the default and the best possible BM performance, showing how dynamically changing the parameter values improves PEPT algorithms. The method of comparison between the PEPT-detected trajectories and the GATE-prescribed trajectory is the same as in Section 2.3.2.

3. Results and discussion

3.1. Model validation results

Each of the static tracer experiments described in Sections 2.1 and 2.2 produce a unique amount of attenuation. Some of the coincident 511 keV gamma-rays attenuated via Compton scattering are inadvertently passed to the PEPT algorithm as corrupted LoRs. When the attenuating medium is air, the amount of corrupted LoRs is relatively low, but as the medium becomes more attenuating, a larger fraction of LoRs are corrupted. This is clearly shown in Fig. 9 where the LoRs from the air, glass, and copper attenuation experiments are plotted.

Since these materials produce different fractions of corrupted LoRs, the optimal f for each experiment should be a unique value. The LoRs from the real experiment and simulations were both processed using the BM under a range of f and N_{LoRs} and the variation of the standard deviation in position for different combinations of the two parameters is plotted as colour variation in Fig. 10. These plots show that for static tracers the optimal value of f is decreased when more corrupted LoRs are present and the standard deviation in the position decreases as more N_{LoRs} per sample are used. The experiment and GATE simulations closely agree across all the parameter combinations, both in the optimal values for f and in the standard deviation in the tracer position. For a static tracer, the optimal value for f remains constant and the standard deviation in position will always decrease with greater N_{LoRs}. The optimal values for f across all the materials tested for both the experiment and the simulation are shown in Fig. 11. Additionally, the values for f which minimise the uncertainty are plotted against the fraction of true LoRs in Fig. 12 demonstrating that f must lower when more attenuation occurs. Moreover, this shows that the values for f which minimise position uncertainty are approximately equivalent to the fraction of true LoRs in the sample. This, until now, has been an assumption of the BM, but this provides the first direct evidence that this assumption is true. The experiment and simulation provide similar values in both the overall PEPT precision across all the parameter combinations tested and also the values of f which minimise the uncertainty for a given N_{LoRs}.

Table 2
Comparisons of the experiment and simulation in the optimal parameters for the moving tracer experiment.

Method	Optimal f	Optimal N_{LoRs}
Experiment	0.275	1400
Simulation	0.25	1300
Percent error (%)	−9.09	−7.14

A similar analysis was conducted for the moving tracer experiment. A 22 MBq tracer was fixed to the impeller of an attritor mill and rotated at 100 RPM. In this case, a position error was calculated using Eq. (7) for the experiment and simulation. A range of constant f and N_{LoRs} values are used with the BM to assess the spatial errors produced under different parameter combinations. Trajectories of the experiment and simulation are presented in Fig. 13 showing that the rates of detection are approximately the same. In Fig. 14, the parameter values for f and N_{LoRs} are varied to assess their effect on the spatial error of the reconstructed PEPT trajectory and to find the optimal combination of parameters. The experimental plot has a generally higher error because the error was calculated using fitted functions, assuming perfect circular motion, whereas the GATE simulations benefit from having analytical functions describing the tracer motion. From Fig. 14, the optimal values for f and N_{LoRs} for the real experiment are determined to be 0.275 and 1400, respectively. Similarly, the optimal parameters for the simulation are determined to be 0.25 and 1300, respectively. The optimal parameters and their percent errors are shown in Table 2.

3.2. Applying the Dynamic Birmingham Method to an attritor mill

The GATE simulations of the attritor mill are expanded to test a range of initial particle positions. In a real PEPT experiment on this mill, tracers near the centre of the mill will move slower than tracers

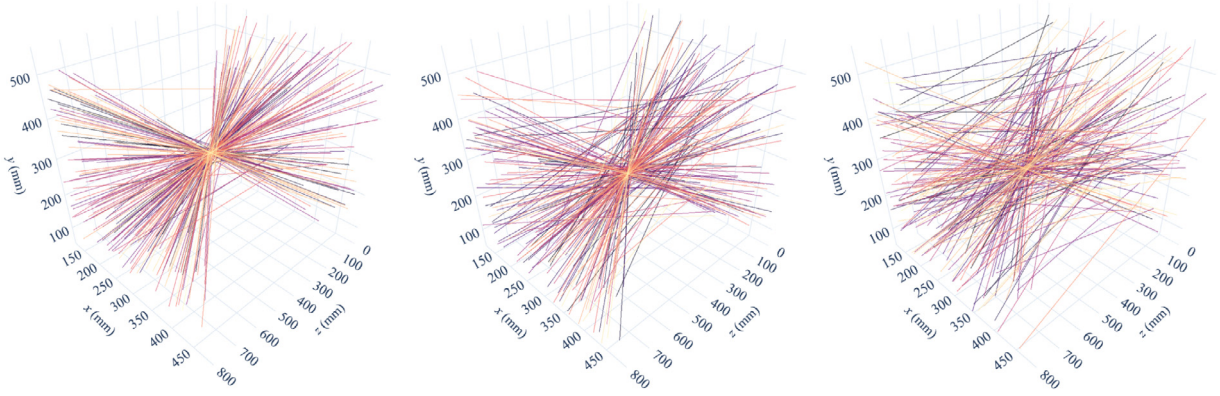

Fig. 9. Three samples of 200 experimentally acquired LoRs from the static tracer experiment for air (left), glass (middle), and copper (right) show that the amount of corrupted LoRs in the sample increases with more attenuation.

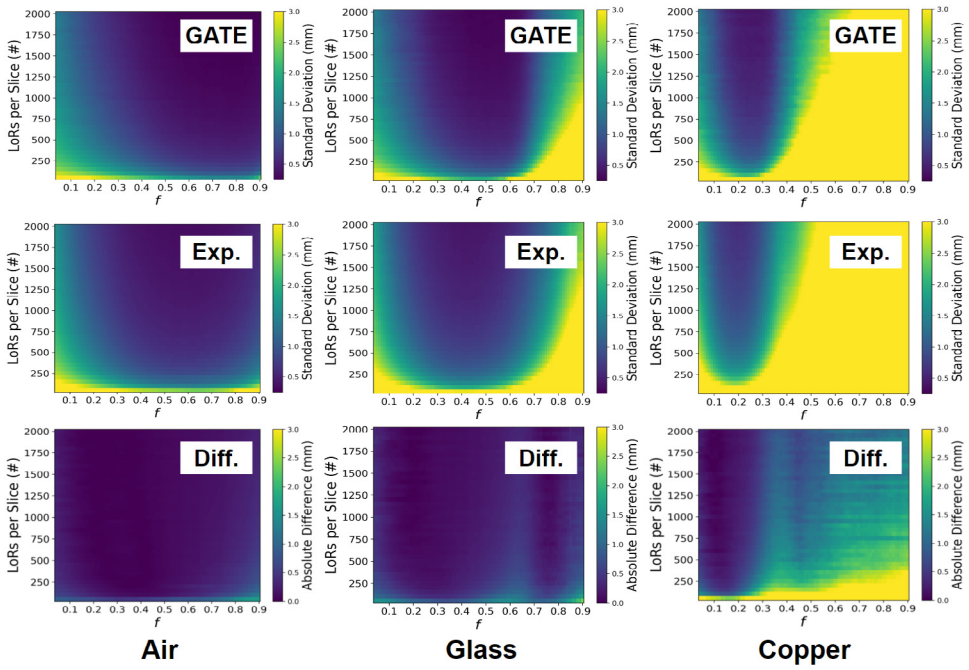

Fig. 10. Position uncertainty in the static tracer experiments and simulations for air (left), glass (middle), and copper (right), and the absolute difference between the simulation and experiment (bottom).

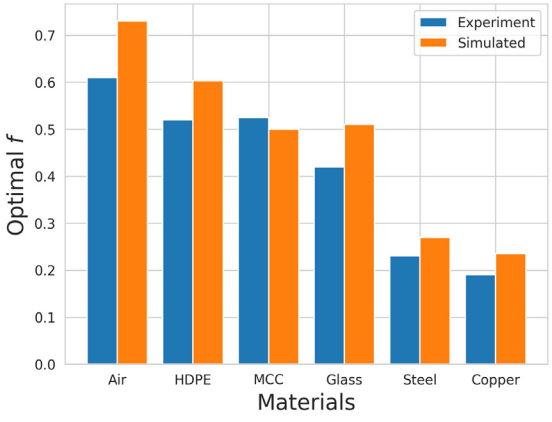

Fig. 11. A comparison of the optimal values for f across all the materials tested.

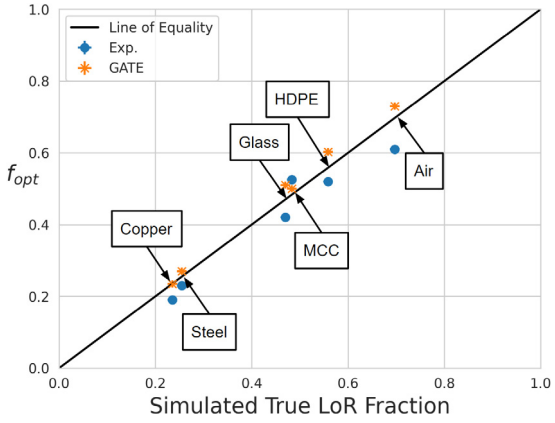

Fig. 12. A comparison of the optimal values for f across all the materials as a function of the fraction of true LoRs in the sample.

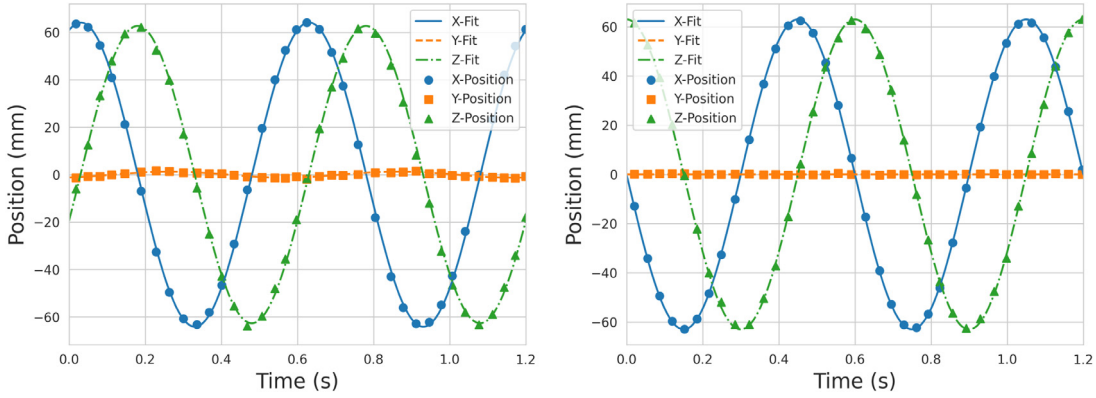

Fig. 13. Trajectories for the experimental tracer in the attritor mill under a constant f of 0.25 and N_{LoRs} of 1500 (left) compared to the simulated tracer trajectory under the same parameters (right).

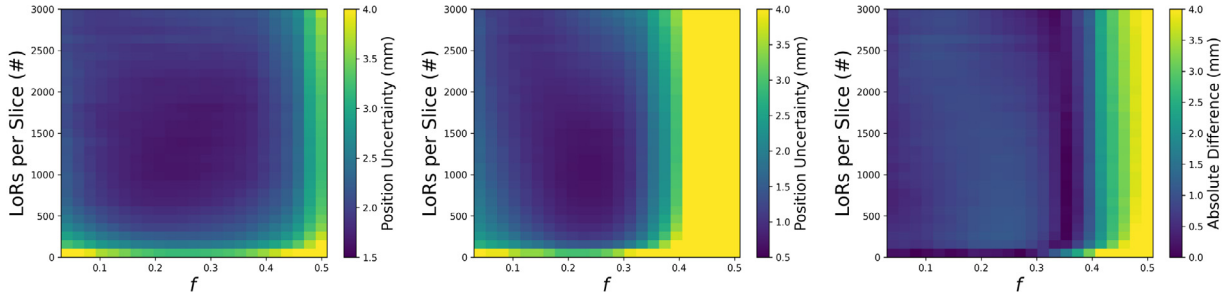

Fig. 14. The parameter values for f and N_{LoRs} are varied for the real experiment (left) and GATE simulation (middle) of the moving source, affecting the spatial error of the reconstructed PEPT trajectory, and the difference between the two is shown (right).

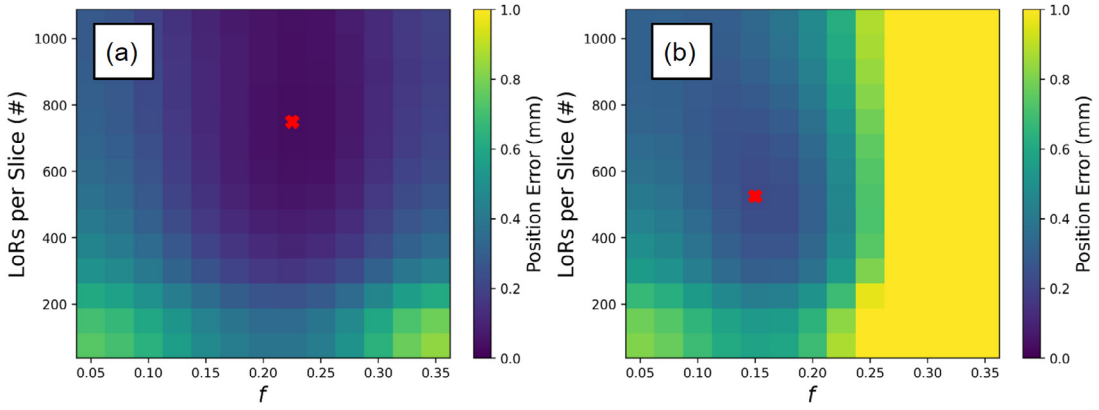

Fig. 15. Panel (a) shows the results of a parameter sweep when the tracer is beside the impeller shaft where the least amount of LoRs have been attenuated while panel (b) shows the effects of the tracer passing behind the impeller shaft where a larger fraction of LoRs are attenuated.

near the tip of the impeller blade, which is where the maximum velocities are recorded [25]. Therefore, the GATE simulated movement of the tracers in this work is similar to that of a real experiment. For each of the tested positions, the optimal values for f and N_{LoRs} were recorded as the tracer moves through the system. These optimal parameters were calculated for every 30° rotation to update their values continuously. Fig. 15 shows the change of optimal parameters at two different degrees of rotation, one where the least amount of attenuation occurs and another where the tracer is behind the impeller shaft, with respect to the detectors, where the most attenuation occurs. As the mill rotates, the optimal parameters fluctuate, becoming more or less conservative when more corrupted events are recorded or the count-rate decreases, such as when the tracer passes in front or behind the impeller shaft.

After the optimal parameters have been extracted, these are used to inform the DBM algorithm. Each simulated trajectory is reprocessed with an estimate of the optimal parameters and the mean spatial error is calculated over the trajectory. These are compared to the trajectories extracted using the default and the best constant parameters. The results of this comparison are in Table 3. The mean spatial error of the default BM parameters, best constant parameters, and the DBM are 2.20 mm, 0.544 mm, and 0.517 mm, respectively. While the default parameters can reconstruct the trajectory, when tailored parameters extracted from Monte Carlo simulation are used, in this case at least, the errors decrease to nearly a quarter of their original values. When dynamic parameters are used, the errors decrease by 76.5% over the default parameters and by 4.03% over the best constant parameters. A histogram of the percent changes in spatial error between the trajectories produced with the best constant parameter and the DBM is shown in Fig. 16. This plot shows the DBM increases the accuracy of nearly all trajectories average and also that some individual trajectories are

Table 3
Mean trajectory comparisons using different algorithm parameter methods.

Parameters	Spatial error (mm)	STD (mm)	Locations (N)
Default	2.20	1.48	1337
Best constant	0.544	0.372	223
Dynamic	0.517	0.3481	236

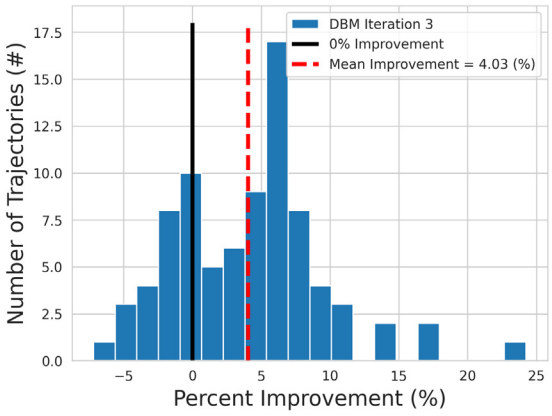

Fig. 16. The change in spatial accuracy for each trajectory. The mean improvement is 4.03% over the best constant parameters.

improved by over 10%. The trajectories which are the most improved are from areas of the system around the impeller blades where the local optimal parameters deviate the most from the best constant parameters.

This work is significant because it demonstrates that the optimal parameter values for the BM can be predicted and that using these improves spatial accuracy over default parameter values. Moreover, not only can the best constant parameter values be estimated, but also the BM can be extended to use the local optimal parameters based on an estimate of the tracer's position, producing the best possible trajectory. In the future, using the methods presented here, Monte Carlo simulations conducted in conjunction with PEPT experiments can be used to remove the guesswork of choosing f and N_{LoRs}. This means users of PEPT algorithms do not need to be experts to produce good trajectories, making the Birmingham Method PEPT algorithm more rigorous and more accessible. While producing simulations of the systems being imaged with PEPT increases the amount of work being done, this work shows that it is worth doing this additional step because of the improvement in trajectories. Additionally, while this work was conducted using the BM PEPT algorithm and the Forte detector system, a similar workflow could be applied to other PEPT algorithms which have free parameters, such as the Feature Point Identification PEPT algorithm, and other detector systems for which a validated Monte Carlo model exists, such as the Phillips Vereos digital photon counting system [32,33].

4. Conclusions

This work shows that the Monte Carlo simulation of PEPT experiments can be used to predict the parameter values of the Birmingham Method PEPT algorithm which provide the best trajectory spatial accuracy. This is demonstrated through experiments and simulations which show that the values for the two key free parameters, f and N_{LoRs}, can be found by comparing the known positions to the reconstructed position and identifying the parameter combination which minimises the spatial error. Further, the values for these parameters are found to be sensitive to the amount of corrupted LoRs in a sample of LoRs and also the velocity and activity of the tracer. For static tracers, the optimal value for f is a balance between removing as many corrupted LoRs as possible while still preserving as many true LoRs and for N_{LoRs} larger values always decrease the spatial error. If too many LoRs are removed (i.e. setting f too low) the spatial error increases due to the statistical uncertainty. Other work has shown uncertainty is proportional to the inverse square root of the number of LoRs remaining in the sample. However, if the tracer is moving, a global optimal combination of f and N_{LoRs} exists. The value for these two parameters is a complex relationship between the amount of corrupted LoRs, tracer velocity, and tracer activity. However, the optimum combination can be found through Monte Carlo simulation of the system and trying a range of parameter value combinations then selecting the one which minimises the spatial error.

Ultimately, the Birmingham Method is extended to update the algorithm parameters on a sample-by-sample basis using the local optimal parameter values. This is demonstrated using a simulation of an attritor mill, representative of a typical PEPT experiment. PEPT trajectories are reconstructed using the Birmingham Method with dynamically updated parameters and compared to trajectories produced with the default and also the best constant parameter combination. In this system, the PEPT trajectory spatial errors are decreased by 76.5% compared to the default parameter and 4.03% compared to the best constant parameters. In light of these results, we suggest that Monte Carlo simulations be used in conjunction with PEPT experiments to determine the algorithm parameters for the Birmingham Method. Doing this removes the guesswork for PEPT users, making the technique more rigorous.

CRediT authorship contribution statement

Matthew Herald: Conceptualization, Methodology, Software, Visualization, Writing – original draft. **Jack Sykes:** Writing – review & editing. **David Parker:** Software. **Jonathan Seville:** Supervision, Writing – review & editing. **Tzany Wheldon:** Resources. **Christopher Windows-Yule:** Supervision, Writing – review & editing.

Declaration of competing interest

The authors declare that they have no known competing financial interests or personal relationships that could have appeared to influence the work reported in this paper.

Data availability

Data will be made available on request.

Acknowledgements

The authors would like to recognise the valuable contributions made by Andrei Leonard Nicuşand for the development of the pept Python package on GitHub and to Dan Rhymer and Mondelez for the use of equipment. The computations described in this paper were performed using the University of Birmingham's BlueBEAR HPC service, which provides a High-Performance Computing service to the University's research community. See theirwebsite for more details. This work was supported by the Engineering and Physical Sciences Research Council, United Kingdom (grant number EP/T034327/1); and the Engineering and Physical Sciences Research Council, United Kingdom Centre for Doctoral Training in Topological Design (grant number EP/S02297X/1). Work at the Positron Imaging Centre is supported in part by a grant from the Engineering and Physical Science Research Council, United Kingdom EP/R045046/1, Probing Multiscale Complex Multiphase Flows with Positrons for Engineering and Biomedical Applications.

References

[1] M. Hawkesworth, D. Parker, P. Fowles, J. Crilly, N. Jefferies, G. Jonkers, Nonmedical applications of a positron camera, Nucl. Instrum. Methods Phys. Res. A 310 (1–2) (1991) 423–434, http://dx.doi.org/10.1016/0168-9002(91)91073-5, URL: https://linkinghub.elsevier.com/retrieve/pii/0168900291910735.

[2] D. Parker, C. Broadbent, P. Fowles, M. Hawkesworth, P. McNeil, Positron emission particle tracking - A technique for studying flow within engineering equipment, Nucl. Instrum. Methods Phys. Res. A 326 (3) (1993) 592–607, http://dx.doi.org/10.1016/0168-9002(93)90864-E, URL: https://linkinghub.elsevier.com/retrieve/pii/016890029390864E.

[3] n. Guobao Wang, High temporal-resolution dynamic PET image reconstruction using a new spatiotemporal kernel method, IEEE Trans. Med. Imaging 38 (3) (2019) 664–674, http://dx.doi.org/10.1109/TMI.2018.2869868.

[4] C. Windows-Yule, J. Seville, A. Ingram, D. Parker, Positron emission particle tracking of granular flows, Annu. Rev. Chem. Biomol. Eng. 11 (1) (2020) annurev–chembioeng–011620–120633, http://dx.doi.org/10.1146/annurev-chembioeng-011620-120633, URL: https://www.annualreviews.org/doi/10.1146/annurev-chembioeng-011620-120633.

[5] C.R.K. Windows-Yule, N. Rivas, D.J. Parker, A.R. Thornton, Low-frequency oscillations and convective phenomena in a density-inverted vibrofluidized granular system, Phys. Rev. E 90 (6) (2014) 062205, http://dx.doi.org/10.1103/PhysRevE.90.062205.

[6] A. Morrison, I. Govender, A. Mainza, D. Parker, The shape and behaviour of a granular bed in a rotating drum using Eulerian flow fields obtained from PEPT, Chem. Eng. Sci. 152 (2016) 186–198, http://dx.doi.org/10.1016/j.ces.2016.06.022.

[7] C. Wiggins, N. Patel, Z. Bingham, A. Ruggles, Qualification of multiple-particle positron emission particle tracking (M-PEPT) technique for measurements in turbulent wall-bounded flow, Chem. Eng. Sci. 204 (2019) 246–256, http://dx.doi.org/10.1016/j.ces.2019.04.030.

[8] D.J. Parker, Positron emission particle tracking and its application to granular media, Rev. Sci. Instrum. 88 (5) (2017) 051803, http://dx.doi.org/10.1063/1.4983046.

[9] W.W. Moses, Fundamental limits of spatial resolution in PET, Nucl. Instrum. Methods Phys. Res. A 648 (2011) S236–S240, http://dx.doi.org/10.1016/j.nima.2010.11.092.

[10] A.H. Compton, A quantum theory of the scattering of X-rays by light elements, Phys. Rev. 21 (5) (1923) 483–502, http://dx.doi.org/10.1103/PhysRev.21.483.

[11] M. Berger, J. Hubbell, S. Seltzer, Z. Chang, J. Coursey, R. Sukumar, D. Zucker, K. Olsen, XCOM: Photon cross sections database, 2009, NIST, URL: https://www.nist.gov/pml/xcom-photon-cross-sections-database.

[12] K. Singh, H. Singh, V. Sharma, R. Nathuram, A. Khanna, R. Kumar, S. Singh Bhatti, H. Singh Sahota, Gamma-ray attenuation coefficients in bismuth borate glasses, Nucl. Instrum. Methods Phys. Res. B 194 (1) (2002) 1–6, http://dx.doi.org/10.1016/S0168-583X(02)00498-6, URL: https://www.sciencedirect.com/science/article/pii/S0168583X02004986.

[13] C. Stearns, D. McDaniel, S. Kohlmyer, P. Arul, B. Geiser, V. Shanmugam, Random coincidence estimation from single event rates on the Discovery ST PET/CT scanner, in: 2003 IEEE Nuclear Science Symposium. Conference Record (IEEE Cat. No.03CH37515), IEEE, Portland, OR, USA, 2004, pp. 3067–3069, http://dx.doi.org/10.1109/NSSMIC.2003.1352545, URL: http://ieeexplore.ieee.org/document/1352545/.

[14] D.J. Parker, D.M. Hampel, T. Kokalova Wheldon, Performance evaluation of the current Birmingham PEPT cameras, Appl. Sci. 12 (14) (2022) 6833, http://dx.doi.org/10.3390/app12146833, URL: https://www.mdpi.com/2076-3417/12/14/6833.

[15] M. Herald, T. Wheldon, C. Windows-Yule, Monte Carlo model validation of a detector system used for positron emission particle tracking, Nucl. Instrum. Methods Phys. Res. A 993 (2021) 165073, http://dx.doi.org/10.1016/j.nima.2021.165073.

[16] S. Jan, G. Santin, D. Strul, S. Staelens, K. Assié, D. Autret, S. Avner, R. Barbier, M. Bardiès, P.M. Bloomfield, D. Brasse, V. Breton, P. Bruyndonckx, I. Buvat, A.F. Chatziioannou, Y. Choi, Y.H. Chung, C. Comtat, D. Donnarieix, L. Ferrer, S.J. Glick, C.J. Groiselle, D. Guez, P.-F. Honore, S. Kerhoas-Cavata, A.S. Kirov, V. Kohli, M. Koole, M. Krieguer, D.J. van der Laan, F. Lamare, G. Largeron, C. Lartizien, D. Lazaro, M.C. Maas, L. Maigne, F. Mayet, F. Melot, C. Merheb, E. Pennacchio, J. Perez, U. Pietrzyk, F.R. Rannou, M. Rey, D.R. Schaart, C.R. Schmidtlein, L. Simon, T.Y. Song, J.-M. Vieira, D. Visvikis, R. Van de Walle, E. Wieërs, C. Morel, GATE - Geant4 Application for Tomographic Emission: A simulation toolkit for PET and SPECT, Phys. Med. Biol. 49 (19) (2004) 4543–4561, URL: https://www.ncbi.nlm.nih.gov/pmc/articles/PMC3267383/.

[17] S. Jan, C. Comtat, D. Strul, G. Santin, R. Trebossen, Monte Carlo simulation for the ECAT EXACT HR+ system using GATE, in: 2003 IEEE Nuclear Science Symposium. Conference Record (IEEE Cat. No.03CH37515), IEEE, 2004, pp. 2545–2548, http://dx.doi.org/10.1109/NSSMIC.2003.1352409, URL: http://ieeexplore.ieee.org/document/1352409/.

[18] D.J. Parker, X. Fan, Positron emission particle tracking—Application and labelling techniques, Particuology 6 (1) (2008) 16–23, http://dx.doi.org/10.1016/j.cpart.2007.10.004.

[19] D. Parker, R. Forster, P. Fowles, P. Takhar, Positron emission particle tracking using the new Birmingham positron camera, Nucl. Instrum. Methods Phys. Res. A 477 (1–3) (2002) 540–545, http://dx.doi.org/10.1016/S0168-9002(01)01919-2, URL: https://linkinghub.elsevier.com/retrieve/pii/S0168900201019192.

[20] T.W. Leadbeater, D.J. Parker, J. Gargiuli, Positron imaging systems for studying particulate, granular and multiphase flows, Particuology 10 (2) (2012) 146–153, http://dx.doi.org/10.1016/j.partic.2011.09.006.

[21] R. Yao, J. Cadorette, J.-F. Beaudoin, R. Lecomte, Energy window optimization of PET detectors for SPECT imaging, in: 2013 IEEE Nuclear Science Symposium and Medical Imaging Conference, 2013 NSS/MIC, 2013, pp. 1–4, http://dx.doi.org/10.1109/NSSMIC.2013.6829104.

[22] C.R.K. Windows-Yule, M. Herald, L. Nicusan, C. Wiggins, G. Pratx, S. Manger, E.A. Odo, T. Leadbeater, J. Pellico, R. de Rosales, A. Renaud, I. Govender, L. Carasik, A. Ruggles, T. Kokalova-Wheldon, J. Seville, D.J. Parker, Recent advances in positron emission particle tracking: A comparative review, Rep. Progr. Phys. (2021) http://dx.doi.org/10.1088/1361-6633/ac3c4c, URL: https://iopscience.iop.org/article/10.1088/1361-6633/ac3c4c.

[23] M. Herald, J. Sykes, D. Werner, J. Seville, C. Windows-Yule, DEM2gate: Combining discrete element method simulation with virtual positron emission particle tracking experiments, Powder Technol. (2022) 117302, http://dx.doi.org/10.1016/j.powtec.2022.117302, URL: https://linkinghub.elsevier.com/retrieve/pii/S0032591022001966.

[24] Y. Yang, N.A. Rowson, R. Tamblyn, A. Ingram, Effect of operating parameters on fine particle grinding in a vertically stirred media mill, Sep. Sci. Technol. 52 (6) (2017) 1143–1152, http://dx.doi.org/10.1080/01496395.2016.1276931.

[25] D. Daraio, J. Villoria, A. Ingram, A. Alexiadis, E. Hugh Stitt, M. Marigo, Validation of a Discrete Element Method (DEM) model of the grinding media dynamics within an attritor mill using Positron Emission Particle Tracking (PEPT) measurements, Appl. Sci. 9 (22) (2019) 4816, http://dx.doi.org/10.3390/app9224816, URL: https://www.mdpi.com/2076-3417/9/22/4816.

[26] K. Cole, D.J. Barker, P.R. Brito-Parada, A. Buffler, K. Hadler, I. Mackay, D. Mesa, A.J. Morrison, S. Neethling, A. Norori-McCormac, B. Shean, J. Cilliers, Standard method for performing positron emission particle tracking (PEPT) measurements of froth flotation at PEPT Cape Town, MethodsX 9 (2022) 101680, http://dx.doi.org/10.1016/j.mex.2022.101680, URL: https://www.sciencedirect.com/science/article/pii/S2215016122000644.

[27] S. Jan, G. Santin, D. Strul, S. Staelens, K. Assié, D. Autret, S. Avner, R. Barbier, M. Bardiès, P.M. Bloomfield, et al., GATE: A simulation toolkit for PET and SPECT, Phys. Med. Biol. 49 (19) (2004) 4543–4561, http://dx.doi.org/10.1088/0031-9155/49/19/007.

[28] M. Herald, Z. Bingham, R. Santos, A. Ruggles, Simulated time-dependent data to estimate uncertainty in fluid flow measurements, Nucl. Eng. Des. 337 (2018) 221–227, http://dx.doi.org/10.1016/j.nucengdes.2018.07.005, URL: https://linkinghub.elsevier.com/retrieve/pii/S0029549318303844.

[29] S. Kerhoas-Cavata, D. Guez, Modeling electronic processing in GATE, Nucl. Instrum. Methods Phys. Res. A 569 (2) (2006) 330–334, http://dx.doi.org/10.1016/j.nima.2006.08.107.

[30] S. Usman, A. Patil, Radiation detector deadtime and pile up: A review of the status of science, Nucl. Eng. Technol. 50 (7) (2018) 1006–1016, http://dx.doi.org/10.1016/j.net.2018.06.014, URL: https://linkinghub.elsevier.com/retrieve/pii/S1738573318302596.

[31] D. Parker, D. Allen, D. Benton, P. Fowles, P. McNeil, M. Tan, T. Beynon, Developments in particle tracking using the Birmingham Positron Camera, Nucl. Instrum. Methods Phys. Res. A 392 (1–3) (1997) 421–426, http://dx.doi.org/10.1016/S0168-9002(97)00301-X, URL: https://linkinghub.elsevier.com/retrieve/pii/S016890029700301X.

[32] C. Wiggins, R. Santos, A. Ruggles, A feature point identification method for positron emission particle tracking with multiple tracers, Nucl. Instrum. Methods Phys. Res. A 843 (2017) 22–28, http://dx.doi.org/10.1016/j.nima.2016.10.057, URL: https://www.sciencedirect.com/science/article/pii/S0168900216311184.

[33] J. Salvadori, J. Labour, F. Odille, P.-Y. Marie, J.-N. Badel, L. Imbert, D. Sarrut, Monte Carlo simulation of digital photon counting PET, EJNMMI Phys. 7 (1) (2020) 23, http://dx.doi.org/10.1186/s40658-020-00288-w.